AD-A260 702

KEEP THIS COPY FOR REPRODUCTION PURPOSES

DOCUMENTATION PAGE

Form Approved
OMB No. 0704-0188

1. AGENCY USE ONLY (Leave blank)	2. REPORT DATE	3. REPORT TYPE AND DATES COVERED
	November, 1992	Technical Report 11/1/91-10/31/92

4. TITLE AND SUBTITLE
"Shear Band Formation in a W-Ni-Fe Alloy under Plate Impact"

5. FUNDING NUMBERS
DAAL03-91-G-0025

6. AUTHOR(S)
M. Zhou, R.J. Clifton, and A. Needleman

7. PERFORMING ORGANIZATION NAME(S) AND ADDRESS(ES)
Division of Engineering, Box D
BROWN UNIVERSITY
Providence, RI 02912
Att: R.J. Clifton, P.I.

8. PERFORMING ORGANIZATION REPORT NUMBER
None

9. SPONSORING / MONITORING AGENCY NAME(S) AND ADDRESS(ES)
U. S. Army Research Office
P. O. Box 12211
Research Triangle Park, NC 27709-2211

10. SPONSORING / MONITORING AGENCY REPORT NUMBER
ARO 28575.1-MS

11. SUPPLEMENTARY NOTES
The view, opinions and/or findings contained in this report are those of the author(s) and should not be construed as an official Department of the Army position, policy, or decision, unless so designated by other documentation.

12a. DISTRIBUTION / AVAILABILITY STATEMENT
Approved for public release; distribution unlimited.

12b. DISTRIBUTION CODE

13. ABSTRACT *(Maximum 200 words)*

A thin foil of a W-Ni-Fe alloy, 50-200μm in thickness, is sheared for 2μs under plane wave conditions by plate impact. Shear bands observed show more intensely localized deformations than obtained in other experiments. The responses of the constituent phases, the tungsten grains and the matrix, as well as that of the composite alloy over a strain rate range of $10^{-4}s^{-1}$ to $7 \times 10^{5}s^{-1}$ are experimentally obtained and characterized by a viscoplastic model. The effects of strain hardening, thermal softening, material inertia, rate sensitivity, heat conduction and material microscopic inhomogeneity, on dynamic shear localization, are investigated through finite element simulations.

93-03146

14. SUBJECT TERMS	15. NUMBER OF PAGES
shear bands, adiabatic shear bands, WHA, tungsten heavy alloys, plate impact, pressure-shear impact	14
	16. PRICE CODE

17. SECURITY CLASSIFICATION OF REPORT	18. SECURITY CLASSIFICATION	19. SECURITY CLASSIFICATION OF ABSTRACT	20. LIMITATION OF ABSTRACT
UNCLASSIFIED	UNCLASSIFIED	UNCLASSIFIED	UL

SHEAR BAND FORMATION IN A W-Ni-Fe ALLOY UNDER PLATE IMPACT

M. Zhou, R. J. Clifton and A. Needleman
Division of Engineering
Brown University
Providence, RI 02912

A thin foil of a W-Ni-Fe alloy, $50 - 200\mu m$ in thickness, is sheared for $2\mu s$ under plane wave conditions by plate impact. Shear bands observed show more intensely localized deformations than obtained in other experiments. The responses of the constituent phases, the tungsten grains and the matrix, as well as that of the composite alloy over a strain rate range of $10^{-4}s^{-1}$ to $7 \times 10^{5}s^{-1}$ are experimentally obtained and characterized by a viscoplastic model. The effects of strain hardening, thermal softening, material inertia, rate sensitivity, heat conduction and material microscopic inhomogeneity, on dynamic shear localization, are investigated through finite element simulations.

Introduction

The performance of tungsten heavy alloys (WHA) in impact applications has been understood to depend strongly on its resistance to the formation of shear bands. The resulting reduction in performance as a penetrator is associated with excessive mushrooming of the projectiles. Understanding the mechanisms through which shear strain localizes in these alloys is therefore important for improving the performance through revisions in materials design and processing. The combination of high density, high strength and toughness that the alloys possess results from the composite microstructure of hard tungsten grains in a ductile matrix, such as the nickle-iron-tungsten (Ni-Fe-W) matrix used for the alloy studied in the current investigation.

To better understand the performance in impact applications it is necessary to characterize the material behavior under such high rate dynamic conditions. The mechanical properties of these alloys have traditionally been studied by means of tensile and compressive tests at quasi-static or low strain rate conditions, Churn and German (1984)[1], O'Donnell and Woodward (1990)[2], Rabin and German (1988)[3], Krock and Shepard (1963)[4] and Krock (1964)[5]. Woodward, Baldwin, Burch and Baxter (1985)[6] studied the effect of strain rate in the range of $10^{-3}s^{-1}$ to $10^{3}s^{-1}$ on the flow stress of three liquid phase sintered tungsten heavy alloys under compression. They reported a slow increase of flow stress with increasing strain rate. Thermal softening was observed for strain rates greater than $2\ s^{-1}$. Coates and Ramesh (1990a,1990b, 1992)[7-9] found approximately a 25% increase in the flow stress, at a strain of 8% over the strain rate range of $1 \times 10^{-4}s^{-1}$ to $7 \times 10^{3}s^{-1}$ in alloys containing 90% to 97% W. They used compressional and torsional Kolsky bars. Increasing strength and decreasing ductility with increasing strain rates in tensile and compression tests have also been reported by Meyer, Kunze, and Staskewitsch (1983)[10].

Shear band formation has been observed in torsional Kolsky bar tests by Andrews, Bower and Duffy (1992)[11] and Weerasooriya and co-workers (1992)[12]. Shear bands observed

under their test conditions have an average width of about $100\mu m$. Andrews *et al* (1992)[11] found that the peak temperature in the shear band is about 580^0C and axial pressures delay the process of shear band formation.

The need to understand the material response at even higher strain rates (up to $10^6\ s^{-1}$) and under pressures found in impact applications motivates the current study. Pressure-shear plate impact (Clifton and Klopp, 1985)[13] provides an ideal means for this purpose.

The Materials

Figure 1 shows the microstructure of a $93\% - W$, $4.9\% - Ni$ and $2.1\% - Fe$ heavy alloy before test. This is a typical structure for such an alloy, consisting of tungsten grains connected by a matrix phase of tungsten, nickel and iron. In order to understand the effects of material inhomogeneity on the alloy's behavior, we determine the responses of the two distinct phases as well as that of the composite. To this end pure tungsten and an alloy custom-made to match the the reported compositions of the matrix phase (Ekbom, 1981[14], O'Donnell and Woodward, 1990[2], Hofman and Petzow, 1984[15]) are studied along with the tungsten alloy. Table 1 shows the compositions and processing states of the three materials used. Both the WHA and the matrix alloy are cross-rolled to a thickness reduction of 8% in each direction after sintering. An as-sintered WHA with the same nominal composition and preparation is also used to study the effect of post-sintering deformation on the dynamic behavior. The pure tungsten was compacted by isostatic pressing at a pressure of $270MPa$, sintered in a dry hydrogen atmosphere at 2100^0C for 30 hours, warm forged and heat-treated at 1200^0C for 1 hour (Lassila and Connor, 1991)[16].

Pressure-Shear Plate Impact Experiment

The configuration of the pressure-shear plate impact experiment is shown in Figure 2, as described by Clifton and Klopp, (1985)[13]. The experiment involves the shearing of a thin foil specimen sandwiched between two hard tungsten carbide plates. The specimen, which is carefully lapped to thicknesses between 50 μm and 100 μm, is subjected to simple shear for 2 μs at nominal shear strain rates between 10^5 and $10^6\ s^{-1}$, under pressures of the order of 10 GPa. Plane wave loading is achieved by the impact of the thin specimen, bonded to the front of a tungsten carbide flyer plate, with a stationary anvil plate. Combined pressure and shear loading is obtained by having the parallel impact faces inclined relative to the direction of approach. The impact is achieved on a 2.5" gas gun whose test chamber is evacuated to vacuum levels of about 100×10^{-6} torr during experiments. The transverse and normal particle velocity components, V_{fs} and U_{fs}, at the rear surface of the anvil plate, are measured with a combined normal velocity and transverse displacement interferometer system (Kim, Clifton and Kumar, 1977)[17]. The shear stress τ, normal pressure on the specimen p and nominal shear strain rate $\dot{\gamma}$ are obtained from V_{fs} and U_{fs} by means of the relations

$$\tau = \frac{1}{2}(\rho c_2)V_{fs}, \quad p = \frac{1}{2}(\rho c_1)U_{fs}; \tag{3.1}$$

$$\dot{\gamma} = \frac{V_0 \sin\vartheta - V_{fs}}{h}, \tag{3.2}$$

where ρc_1 and ρc_2 are the normal and shear impedances of the anvil plate respectively; V_0 is the projectile velocity; θ is the skew angle of the specimen; and h is the initial thickness of the specimen. The shear strain rate is integrated to yield the shear strain

$$\gamma(t) = \int_0^t \dot{\gamma}(\tau) d\tau. \tag{3.3}$$

This experiment provides the simplicity of allowing the onset of shear localization and the development of a shear band to be interpreted from the stress-time and stress-strain profiles for the plane wave loading, under conditions for which the pressure history is well known. Because of the high normal pressure applied to the specimen this configuration provides a condition in which the effects of pressure on shear band formation can be investigated. Since there are no free surfaces shear band initiation and development are independent of a macroscopic geometrical defect parameter, which is important in analyses concerning other experimental configurations, such as the torsional Kolsky bar test, Molinari and Clifton (1987)[18]. Table 2 summaries the pressure-shear experiments on WHA, the matrix alloy and W.

Torsional Kolsky Bar Tests

In order to obtain material response over a wide range of strain rates, we have conducted torsional Kolsky bar tests on the matrix alloy. In addition, data from similar tests by Andrews *et al* (1992)[11] on a similar W-Ni-Fe alloy containing 93% W are used along with pressure-shear impact results to obtain a complete understanding of the behaviors of the WHA and the matrix alloy. Quasi-static torsional tests are also conducted on the torsional Kolsky bar apparatus with minor modifications. The configuration of this experiment has been described by Duffy and co-workers, Hartley *et al* (1985)[19], Duffy *et al* (1971)[20] and Costin *et al* (1979)[21]. In this test the tube gauge section of the specimen is subjected to torsional deformation at shearing strain rates of the order of $10^3 s^{-1}$. The torsional loading is achieved by clamping the specimen between two aluminum bars and suddenly releasing a torque stored in the incident bar. Torsional pulses up to $600\mu s$ in duration can be generated. Instantaneous shear stress and nominal shear strain rate are obtained by measuring respectively the transmitted pulse strength in the transmitter bar and the reflected pulse strength in the incident bar. Shear strain is subsequently obtained by a simple integration of the shear strain rate.

Table 3 shows the torsional Kolsky bar tests conducted on the matrix alloy. Tests at elevated temperatures of 200^0C and 250^0C are conducted to gain information on the temperature dependence of the stress-strain curves.

Experimental Results

Figure 3 shows the stress-strain curves for the WHA at different strain rates obtained by pressure-shear impact, torsional Kolsky bar and quasi-static torsion. The results from the Kolsky bar and quasi-static torsion tests are obtained by Andrews *et al* (1992)[11]. The alloy shows strain hardening at $\dot{\gamma} \sim 10^{-4} s^{-1}$. The dynamic curves on the other hand show apparent softening of the material. This is attributed to the material thermal softening

resulting from the heat generated by the plastic deformation. Two Kolsky bar tests are shown. The defect parameter ϵ, which is defined as the tube wall thickness variation in the specimen gauge section, apparently has a strong influence on the critical strain for shear localization. Figure 4 shows the deformed microstructure of the specimen after pressure-shear impact. No shear band is observed in this particular shot (Shot 9201).

As the amount of shear strain is increased by reducing the specimen thickness, increasing the impact velocity and increasing the impact angle, shear bands form in the specimen. Figure 5 shows the stress-strain curves from three shots involving specimens $57 - 87\mu m$ in thickness and impact angles of $18 - 26.6^0$. Shear bands are observed in the two higher angle shots (Shots 9206 and 9211). Critical nominal shear strains at the onset of shear localization are between $1 - 1.5$. These values are significantly higher than what is shown in Figure 3 for Kolsky bar tests. Figure 6 shows the shear band morphologies in Shots 9206 and 9211. The intensely sheared region involves both the W gains and the matrix. The shear bands are $5 - 10\mu m$ in width compared with the reported values of about $100\mu m$ in Kolsky bar tests, Andrews *et al* (1992)[11].

Figure 7 shows the flow stress dependence on logarithmic shear strain rate. The WHA shows a strong rate sensitivity. Figure 8 compares the dynamic stress-strain curves of the as-sintered WHA, cross-rolled WHA and pure tungsten. This figure shows that the flow stress of the WHA is increased by the post-sintering mechanical working. The stress level of the cross-rolled WHA is essentially the same as that of the pure tungsten.

Figure 9 is a summary of the responses for the matrix alloy under different strain rates. The quasi-static tensile curve is obtained by Penrice (1992)[22]. Unlike the WHA, the matrix alloy shows strain hardening at both quasi-static and dynamic conditions. This indicates that the softening due to plastic dissipation is relatively small and insufficient to overcome the strain hardening effect under the test conditions. This lack of strain softening can be explained as follows. While the matrix alloy has a specific heat three times that of the WHA, its flow stress is only about one half that of the WHA. For the same amount of plastic strain the temperature change would likely be only one third of that for the heavy alloy, considering a factor of two difference in the densities. The strain rate sensitivity of the matrix alloy is shown in Figure 7. The flow stresses plotted correspond to a shear strain of $\gamma = 0.45$. It should be noted that the matrix alloy exhibits a lower rate dependence of the flow stress than the WHA.

Figure 10 shows the torsional dynamic stress-strain curves for the matrix alloy at room temperature, 200^0C and 250^0C. The temperature dependence of flow stresses for WHA, the matrix alloy and pure W are summarized in Figure 11. The data for WHA are reported by Andrews *et al* (1992)[11], Bose, Sims and German (1988)[23], and O'Donnell and Woodward (1990)[2]. The solid lines are model predictions. It is assumed that the materials lose stress carrying capacity when the temperature reaches their corresponding melting points.

Material Behavior Characterization

Over the range of strain rates from 10^{-4} s^{-1} to 3.0×10^3 s^{-1} the material response can

be characterized by an empirical visco-plastic constitutive relation of the form

$$\dot{\gamma}_1 = \dot{\gamma}_0 \Big[\frac{\tau}{g(\gamma^p, T)}\Big]^m, \tag{6.1}$$

where $\dot{\gamma}_1$ is the shear strain rate, τ is the shear stress, $\dot{\gamma}_0$ is a reference strain rate, m is a rate sensitivity parameter and

$$g(\gamma^p, T) = \tau_0 (1 + \gamma^p/\gamma_0)^n \Big\{1 - \beta\Big[(T/T_0)^\kappa - 1\Big]\Big\}, \tag{6.2}$$

represents the stress-strain relation at a constant shear strain rate of $\dot{\gamma} = \dot{\gamma}_0$ and at constant temperature T. In Eqn. (6.2), γ^p is the plastic shear strain, τ_0 is a reference shear stress, γ_0 is a reference shear strain, n is the strain hardening exponent; T_0 is a reference temperature; β and κ are thermal softening parameters which are determined by fitting the available data shown in Figure 11.

In order to account for the behavior at higher strain rates the relation (6.1) is modified to

$$\dot{\gamma}^p = \frac{\dot{\gamma}_1 \dot{\gamma}_2}{\dot{\gamma}_1 + \dot{\gamma}_2}, \tag{6.3}$$

where $\dot{\gamma}^p$ is the plastic shear strain rate and

$$\dot{\gamma}_2 = \dot{\gamma}_m \exp\Big[-\frac{\alpha g(\gamma^p, T)}{\tau}\Big], \tag{6.4}$$

is a mathematical model of the limiting viscoplastic response at very high strain rates. In Eqn. (6.4) α is a strain rate sensitivity parameter for strain rates above, say, 3×10^3 s^{-1}. The form (6.3) limits the strain rate to values less than $\dot{\gamma}_m$. It also provides a smooth transition between the measured response $\dot{\gamma}^p = \dot{\gamma}_1(\tau, \gamma^p)$ at strain rates less than, say, 10^3 s^{-1}, and the limiting behavior $\dot{\gamma}^p = \dot{\gamma}_2(\tau, \gamma^p)$ at strain rates greater than, say, 10^5 s^{-1}. The value of $\dot{\gamma}_m$ is not available from experiments; a value of 8×10^8 s^{-1} is chosen, primarily for the numerical purpose of avoiding the need for unreasonably small time steps at early times when the shear stresses are large.

The behavior of the matrix alloy can be adequately described by a single relation of the form $\dot{\gamma}^p = \dot{\gamma}_1(\tau, \gamma^p)$ for the whole strain range studied. The model parameters for the cross-rolled WHA, matrix alloy and pure tungsten are listed in Table 4.

Finite Element Simulations

The phenomenon of dynamic shear strain localization is a coupled thermo-mechanical process that involves the effects of strain hardening, material inertia, rate dependence, thermal softening and heat transfer. Simulation of the experiments requires solving the coupled thermal and mechanical field equations. The finite element simulation is based on a finite deformation formulation by Needleman (1989)[24]. The formulation employs a convected coordinate, Lagrangian expression of the field equations. A material point **y** initially at **x** in the

reference configuration assumes a position $\bar{\mathbf{x}}$ in the current configuration. The displacement vector $\mathbf{u}$ and the deformation gradient tensor are defined by

$$\mathbf{u} = \bar{\mathbf{x}} - \mathbf{x}, \qquad \mathbf{F} = \frac{\partial \bar{\mathbf{x}}}{\partial \mathbf{x}}. \tag{7.1}$$

The dynamic principle of virtual work is written as

$$\int_V \tau^{ij} \delta E_{ij} dV = \int_S T^i \delta u_i dS - \int_V \rho \frac{\partial^2 u^i}{\partial t^2} \delta u_i dV, \tag{7.2}$$

where V, S and ρ are the volume, surface and mass density, respectively, of the body in the reference configuration, and τ^{ij} are the contravariant components of Kirchhoff stress on the deformed convected coordinates. Also, $T^i = (\tau^{ij} + \tau^{kj} u^i_{,k}) n_j$, are the tractions on a surface in the reference configuration and $E_{ij} = \frac{1}{2}(u_{i,j} + u_{j,i} + u^k_{,i} u_{k,j})$, are components of the Lagrangian strain. In the equations above, n_j are the components of the reference surface normal $\mathbf{n}$; and $()_{,i}$ denotes differentiation in the reference frame.

The heat equation, based on the dependence of heat flux on the temperature gradient across a surface in the current configuration, is written as, (Povirk, 1992)[25]

$$\rho c_p \dot{T} = \chi \boldsymbol{\tau} : \mathbf{d}^p + Jk \nabla_{\mathbf{x}} \cdot (\mathbf{F}^{-1} \mathbf{F}^{-T} \nabla_{\mathbf{x}} T), \tag{7.3}$$

where c_p is the specific heat; $\chi = 0.9$ is the portion of plastic work converted to heat; T is the temperature; $\mathbf{d}^p$ is the plastic rate of deformation tensor; $J = det\,|\mathbf{F}|$; k is the heat conductivity; $\nabla_{\mathbf{x}}$, $()^{-1}$ and $()^{-T}$ denote, respectively, $\frac{\partial}{\partial \mathbf{x}}$, inverse and inverse transpose. The variational equation used for finite element discretization can be obtained by multiplying Eqn (7.3) by δT, an arbitrary variation in admissible temperature fields, and integrating over the reference volume

$$\begin{aligned} \int_V \rho c_p \dot{T} \delta T dV = & \int_V \chi \boldsymbol{\tau} : \mathbf{d}^p \delta T dV + \int_S k(\mathbf{F}^{-1} \mathbf{F}^{-T} \nabla_{\mathbf{x}} T) \cdot \mathbf{n} \delta T dS \\ & - \int_V k(\mathbf{F}^{-1} \mathbf{F}^{-T} \nabla_{\mathbf{x}} T) \cdot (\nabla_{\mathbf{x}} \delta T) dV. \end{aligned} \tag{7.4}$$

Finite element discretization of the dynamic principle of virtual work and the variational heat equation yields respectively

$$M \frac{\partial^2 U}{\partial t^2} = F, \tag{7.5}$$

and

$$C \frac{\partial T}{\partial t} = -KT + H, \tag{7.6}$$

where M, U and F are the mass matrix, nodal displacement and nodal force vectors respectively. C and K are, respectively, the heat capacitance and heat conductance matrices; H is the thermal force vector. Lumped mass and heat capacitance matrices are used in the implementation to obtain explicit algorithms for solving the coupled systems of equations.

Discussion

Both one- and two-dimensional simulations are conducted to investigate the effects of material inertia, heat conduction and material microcopic inhomogeneity on the shear band formation. By considering the WHA as a uniform continuum, one-dimensional simulation of the pressure-shear impact experiment is possible. This provides a means for studying the roles of dynamic wave propagation and heat conduction in determining the onset and location of the shear band. Figures 12-15 show the calculated results for Shot 9206. The distributions of plastic strain, strain rate and temperature at different times show that shear localization starts at about $1.6\mu s$ after impact. The shear band is located approximately $25\mu m$ from the impact face. Experiments and computations show that the competition between the thermal softening due to plastic dissipation and the stabilizing effect of heat conduction causes the shear band to form away from the impact face. The calculated shear band width is about $5\mu m$, which agrees well with that observed in experiments, Figure 6. The peak temperature inside the shear band reaches about 1300 K, which is significantly higher than the value reported in torsional Kolsky bar tests by Andrews *et al* (1992)[11]. The higher value in the pressure-shear configuration is due to the more intense shear deformation in the narrower shear band. It is also clear from Figure 13 that material outside the shear band experiences practically no plastic deformation shortly after the onset of the shear localization.

The effect of microscopic material inhomogeneity is considered by modeling the material as a composite of an array of cylindrical tungsten grains connected by a matrix binder phase. The tungsten grains have high density, high flow stress, high melting temperature, low rate of strain hardening and low specific heat while the matrix has lower density, lower flow stress, lower melting temperature, higher rate of strain hardening and higher specific heat. Figure 16 shows the undeformed structure of the simulated composite. The cylindrical grains are $28\mu m$ in diameter. The deformed configuration at $2\mu s$ after impact is shown in Figure 17. The deformed structures of the grains and the matrix are shown separately for clarity. A band involving both the W grains and the matrix phase forms through the middle section. The band width is between $5-10\mu m$. The maximum equivalent plastic strain inside the band is approximately 12. The shapes of the deformed grains are comparable to those observed in the experiments.

Conclusions

Pressure-shear plate impact is used to study the dynamic formation of shear bands in a tungsten heavy alloy. The experiment subjects the material to simple shear under shearing strain rates up to $7 \times 10^5\ s^{-1}$. Dynamic stress-strain relations obtained from torsional Kolsky bar tests and the pressure-shear impact tests show that the alloy exhibits significant rate sensitivity and thermal softening due to plastic dissipation. Shear bands form when the plastic strains become sufficiently large. The critical shear strain for shear band development is $4-5$ times that obtained in Kolsky bar tests. This increase is attributed to the insensitivity to macroscopic geometric non-uniformities in the specimen and the effect of hydrostatic pressure on the specimen in the pressure-shear configuration. The conduction of heat plays an important role in determining the location of the shear bands. The experiment provides an opportunity to relate, relatively directly, the shear band development to the

stress-strain and stress-time profiles.

Pressure-shear and torsional tests are conducted to understand the responses of the constituent phases in the alloy, the W grains and the matrix. Experiments on an alloy similar to the matrix phase in composition and microstructure demonstrate that the matrix has a flow strength equal to about one-half that of the WHA. The matrix shows strain hardening for strain rates up to $3.0 \times 10^5\ s^{-1}$, indicating a weak thermal softening rate relative to the strain hardening rate, partly as a result of its high specific heat and lower flow stress compared with the WHA. A weaker stress dependence on strain rate is observed for the matrix. Impact experiments also show that the flow strength of WHA follows that of the tungsten phase and post-sintering deformation significantly strengthens the WHA.

The responses of the WHA, pure tungsten and matrix phase are characterized by a visco-plastic model that incorporates thermal softening based on the experimental data. Applications of the model show that important aspects of the dynamic shear strain localization are reproduced in the simulations.

Significantly more intensely formed shear bands are observed in the pressure-shear impact experiments than those reported in torsional Kolsky bar tests. Finite element simulations considering the effects of finite deformation, material inertia, material viscoplasticity, thermal softening and heat conduction show that the conduction of heat plays an important role in determining the onset of shear localization as well as post-onset deformations in the shear bands. The simulations demonstrate the roles of the two distinct phases in the WHA. The calculations agree well with the experiments in terms of the shear band width, the morphology of the deformed grains in the shear band region, and the critical shear strains.

Acknowledgement

This research is supported primarily by the Army Research Office. The computational work is supported by the NSF MRG on "Micro-Mechanics of Failure-Resistant Materials". Computations were performed at the San Diego Supercomputer Center. We would like to thank Mr. T. W. Penrice of Teledyne Firth Sterling for supplying the tungsten heavy alloy and the matrix alloy, Mr. J. Spencer of GTE for supplying the as-sintered tungsten heavy alloy and Dr. D. H. Lassila of Lawrence Livermore National Laboratory for supplying the pure tungsten used in this investigation. Thanks are extended to M. C. Mello for his assistance in the pressure-shear experiments, G. LaBonte for his assistance in the torsional Kolsky bar tests, and to E. Andrews for making available his results from torsional Kolsky bar tests on the same WHA.

References

1 Churn, K. -S. and German, R. M., (1984), "Fracture Behavior of W-Ni-Fe Heavy Alloys", *Metallurgical Transactions A*, Vol. **15A**, pp. 331-338.

2 O'Donnell, R. G. and Woodward, R. L., (1990), "The Composition and Temperature Dependence of the Mechanical Properties of Tungsten Alloys", *Metallurgical Transactions A*, Vol. **21A**, pp. 744-748.

3 Rabin, B. H. and German, R. M., (1988), "Microstructure Effects on Tensile Properties of Tungsten-Nickle-Iron Composites", *Metallurgical Transactions A*, Vol. **19A**, pp. 1523-1532.

4 Krock, R. H. and Shepard, L. A., (1963), "Mechanical Behavior of the Two-Phase Composite, Tungsten-Nickel-Iron", *Transactions of The Metallurgical Society of AIME*, Vol. **227**, pp. 1127-1134.

5 Krock, R. H., (1964), "Effect of Composition and Temperature on the Dynamic Elastic Moduli of W-Ni-Fe Composite Materials", *Proc. ASTM*, Vol. 64, pp. 712-718.

6 Woodward, R. L., Baldwin, N. J., Burch, I. and Baxter, B. J., (1985), "Effect of Strain Rate on the Flow Stress of Three Liquid Phase Sintered Tungsten Alloys", *Metallurgical Transactions A*, Vol. **16A**, pp. 2031-2037.

7 Coates, R. S. and Ramesh, K. T., (1990a), "The Rate-Dependent Deformation of a Tungsten Heavy Alloy", *The Johns Hopkins University Report*, No. DIL-9001, June, 1990. Baltimore, MD.

8 Coates, R. S. and Ramesh, K. T., (1990b), "The Deformation of Tungsten Alloys at High Strain Rates", *The Johns Hopkins University Report*, No. DIL-9002, November, 1990. Baltimore, MD.

9 Ramesh, K. T. and Coates, R. S., (1992), "Microstructural Influences on the Dynamic Response of Tungsten Heavy Alloys", *Metallurgical Transactions A*, Vol. **23A**, pp. 2625-2630.

10 Meyer, L. W., Kunze, H.-D. and Staskewitsch, E., (1983), "Dynamic Strength and Ductility of a Tungsten-Alloy for KE-Penetrators in Swaged and Unswaged Condition under Various Loading", *Proc. 7th International Symposium on Ballistics*, Hague, pp. 289-293.

11 Andrews, E. W., Bower, A. F. and Duffy, J., (1992), "Shear Band Formation in a Tungsten Heavy Alloy", *manuscript in preparation.*

12 Weerasooriya, T., Beaulieu, P. A. and Swanson, R., (1992), "Deformation and Failure Behavior of 93W-5Ni-2Fe at High Strain Rate Shear Loading", *U. S. Army Materials Technology Laboratory Report*, No. MTL TR 92-19, Watertown, MA.

13 Clifton, R. J. and Klopp, R. W., (1985) "Pressure-Shear Plate Impact Testing", *Metals Handbook*, Vol. 8, Amer. Soc. Metals, Metals Park, 9th ed., pp. 230-239.

14 Ekbom, L., (1981), "Microstructural Study of the Deformation and Fracture Behavior of a Sintered Tungsten-Base Composite", *Modern Developments in Powder Metallurgy*, H. H. Hausner, H. W. Antes and G. D. Smith, eds., Metal Powder Industries Ferderation, Princeton, NJ, Vol. **14**, pp. 177-188.

15 Hofmann, H. and Petzow, G., (1984), "Influence of Sintering Atmosphere on Mechanical Properties of Tungsten Based Heavy Alloys", *Modern Developments in Powder Metallurgy*, Vol. **17**, pp. 17-31.

16 Lassila, D. H. and Connor, A., (1991), "Fracture Behavior of Warm Forged and CVD Tungsten", *Lawrence Livermore National Laboratory Report*, No. UCRL-JC-106552, *Proc. of the Symposium Tungsten Heavy Alloys - Recent Advances*, TMS/AIME Refractory Metals Committee, TMS/AIME 1991 Annual Meeting, New Orleans, Louisiana.

17 Kim, K-S, Clifton, R. J. and Kumar, P., (1977), "A Combined Normal- and Transverse-displacement Interferometer with an Application to Impact of Y-cut Quartz", *J. Applied Physics*, Vol. **48**, No. 10, pp. 4132-4139.

18 Molinari, A. and Clifton, R. J., (1987), "Analytical Characterization of Shear Localization in Thermo-viscoplastic Materials", *Trans. of ASME, J. Appl. Mech.*, Vol. **54**, pp. 806-812.

19 Hartley, K. A., Duffy, J. and Hawley, R. H., (1985), "The Torsional Kolsky (Split-Hopkinson) Bar", *Metals Handbook*, Vol. **8**, ASM, 1985, pp. 218-228.

20 Duffy, J., Campbell, J. D. and Hawley, R. H., (1971), "On the Use of a Torsional Split-Hopkinson Bar to Study Rate Effects in 1100-0 Aluminum", *J. Appl. Mech.*, Vol. **38**, pp. 83-91.

21 Costin, L. S., Crisman, E. E., Hawley, R. H. and Duffy, J., (1979), "On the Localization of Plastic Flow in Mild Steel Tubes under Dynamic Torsional Loading", *Proc. 2nd Conf. on Mech. Properties of Materials at High Rates of Strain*, ed. by J. Harding, The Institute of Physics, London, pp. 90-100.

22 Penrice, T. W., (1992), *Private communication.*

23 Bose, A., and German, R. M., (1990), "Matrix Composition Effects on the Tensile Properties of Tungsten-Molybdenum Heavy Alloys", *Metallurgical Transactions A*, Vol. **21A**, pp. 1325-1327.

24 Needleman, A., (1989), "Dynamic Shear Band Development in Plane Strain", *Journal of Applied Mechanics*, Vol. **56**, pp. 1-9.

25 Povirk, G. L., (1992), "Investigations of Residual Stresses in Al-SiC Composites and Their Effect on Deformation and Damage Behavior", *Brown University Thesis*, Providence, RI.

Table 1 Materials Used in the Study

Material	Supplier	Condition	Composition
WHA	Teledyne Firth Sterling	Cross-Rolled (8% + 8%)	$W-93wt\%$, $Ni-4.9wt\%$ $Fe-2.1\%$
WHA	GTE	AS Sintered	$W-93wt\%$, $Ni-4.9wt\%$ $Fe-2.1\%$
Matrix Alloy	Teledyne Firth Sterling	Cross-Rolled (8% + 8%)	$W-25wt\%$, $Ni-50wt\%$ $Fe-25\%$
W	Lawrence Livermore	Warm Forged	W

Table 2 Pressure-Shear Experiment on WHA, W and Matrix Alloy

Shot #	Specimen Material	Projectile Velocity $mm/\mu s$	Skew Angle θ, °	TDI Constant μm/fringe	Normal Pressure p, MPa	Pressure Change	Shear Stress MPa	Shear Rate $\times 10^5 s^{-1}$	Specimen Thickness μm	Shear Band
9109	WHA(CR)	0.181	21.5	0.8333	8981	No	1100	0.14	1973	No
9201	WHA(CR)	0.188	22.0	0.8333	9326	No	1300	1.2	201	No
9203	WHA(AS)	0.198	21.5	0.8333	9831	No	1160	2.0	175	No
9205	WHA(CR)	0.205	21.5	0.8333	10689	Yes*	1350	3.9	78	Yes
9206	WHA(CR)	0.202	26.6	0.8333	9629	No	1300	5.4	87	Yes
9207	WHA(CR)	0.213	22.0	0.8333	10555	No	1350	4.0	89	Yes
9209	WHA(CR)	0.205	18.0	0.8333	10430	No	1290	3.5	61	No
9211	WHA(CR)	0.205	21.5	0.8333	10174	No	1250	6.5	57	Yes
9204	W(WF)	0.193	22.0	0.8333	9607	No	1340	1.2	195	No
9208	Matrix(CR)	0.200	18.0	0.8333	10146	No	680	3.0	129	No
9212	Matrix(CR)	0.199	21.5	0.8333	9910	No	780	9.0	55	No

CR-Cross Rolled; AS-As Sintered; WF-Warm Forged;

* : High pressure shear window of $1440ns$ followed by low pressure shear window of 520 ns;

Table 3 Dynamic Torsional Tests on Matrix Alloy

Specimen #	Test Temperature $^0C(K)$	Nominal Shear Strain Rate $\times 10^3 s^{-1}$	Flow Stress MPa	Defect Parameter ϵ	Shear Band
M1	250 (523)	1.3	430	0.118	No
M2	RT	0.5	570	0.147	No
M3	200 (473)	1.5	490	0.123	No
M4	RT	1.4	590	0.096	No
M5	RT	1.2	580	0.095	No

Table 4 Model Parameters

WHA(CR)
$\dot{\gamma}_0 = 1.0 \times 10^{-4}\ s^{-1}, \quad m = 40, \quad \tau_0 = 420 MPa$
$\dot{\gamma}_m = 8.0 \times 10^{8}\ s^{-1}, \quad \alpha = 17$
$\gamma_0 = 1.22 \times 10^{-5}, \quad n = 0.05$
$\beta = 2.4, \quad \kappa = 0.2, \quad T_0 = 293\ K$
$k = 120\ W/m \cdot K, \quad c_p = 138\ J/kg \cdot K, \quad \rho = 17700\ kg/m^3$
$E = 3.45 \times 10^{5}\ MPa, \quad \nu = 0.29$
$\bar{\alpha} = 5.3 \times 10^{-6}\ K^{-1}$
Matrix Alloy(CR)
$\dot{\gamma}_0 = 1.0 \times 10^{-4}\ s^{-1}, \quad m = 16, \quad \tau_0 = 58 MPa$
$\gamma_0 = 2.26 \times 10^{-4}, \quad n = 0.20$
$\beta = 2.4, \quad \kappa = 0.20, \quad T_0 = 293\ K$
$k = 100\ W/m \cdot K, \quad c_p = 382\ J/kg \cdot K, \quad \rho = 9200\ kg/m^3$
$E = 2.55 \times 10^{5}\ MPa, \quad \nu = 0.29$
$\bar{\alpha} = 1.5 \times 10^{-5}\ K^{-1}$
W(WF)
$\dot{\gamma}_0 = 1.0 \times 10^{-4}\ s^{-1}, \quad m = 40, \quad \tau_0 = 420 MPa$
$\dot{\gamma}_m = 8.0 \times 10^{8}\ s^{-1}, \quad \alpha = 17$
$\gamma_0 = 1.22 \times 10^{-5}, \quad n = 0.05$
$\beta = 2.4, \quad \kappa = 0.15, \quad T_0 = 293\ K$
$k = 160\ W/m \cdot K, \quad c_p = 138\ J/kg \cdot K, \quad \rho = 19300\ kg/m^3$
$E = 4.00 \times 10^{5}\ MPa, \quad \nu = 0.29$
$\bar{\alpha} = 5.3 \times 10^{-5}\ K^{-1}$

Fig. 1 MICROSTRUCTURE OF CROSS-ROLLED WHA IN THE AS-RECEIVED CONDITION

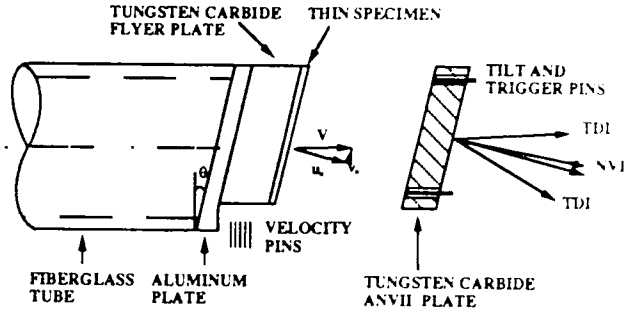

Fig. 2 CONFIGURATION OF PRESSURE-SHEAR PLATE IMPACT EXPERIMENT OF A THIN SPECIMEN

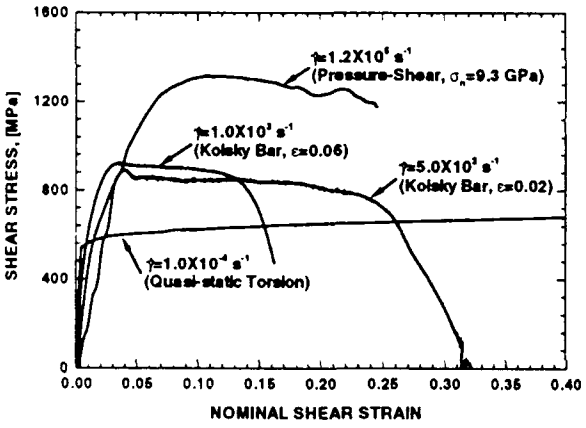

Fig. 3 SHEAR STRESS-STRAIN CURVES OF WHA

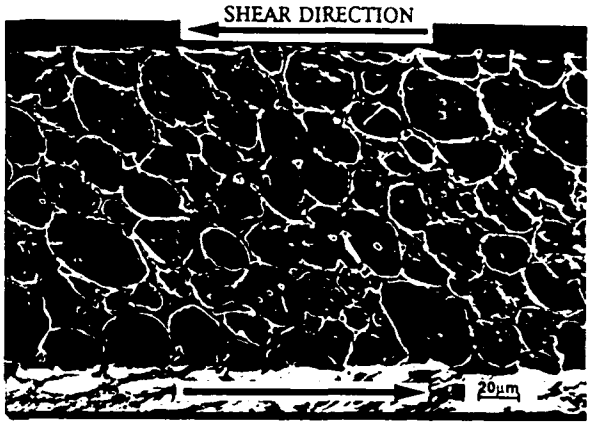

Fig. 4 DEFORMED MICROSTRUCTURE OF WHA AFTER PRESSURE-SHEAR PLATE IMPACT, (Shot 9201)

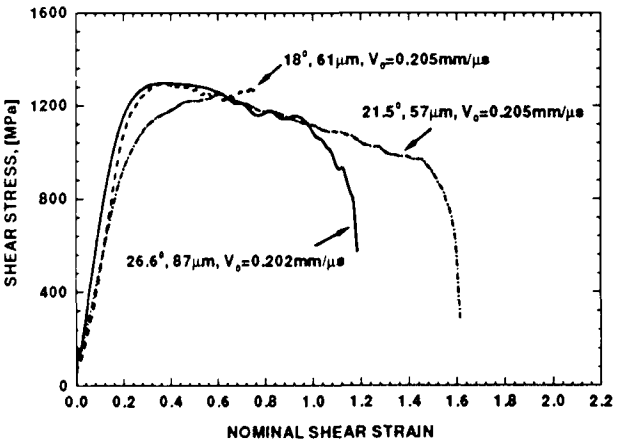

Fig. 5 DYNAMIC SHEAR STRESS-STRAIN CURVES OBTAINED BY PRESSURE-SHEAR PLATE IMPACT

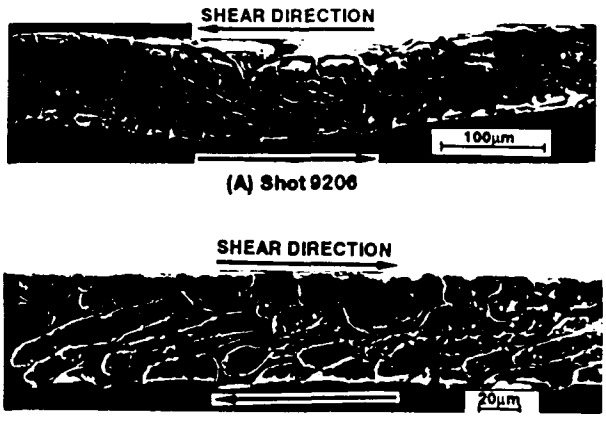

Fig. 6 SHEAR BANDS IN PRESSURE-SHEAR IMPACT EXPERIMENTS

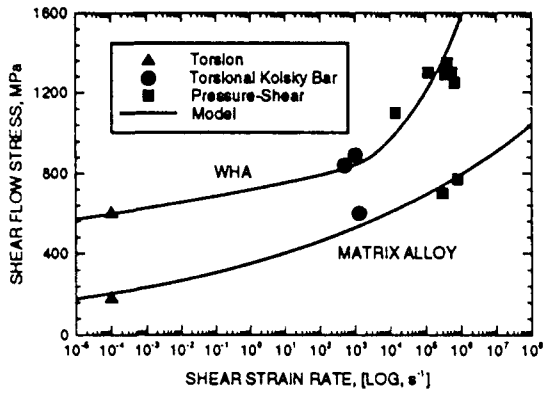

Fig. 7 STRAIN RATE SENSITIVITY OF WHA AND MATRIX ALLOY

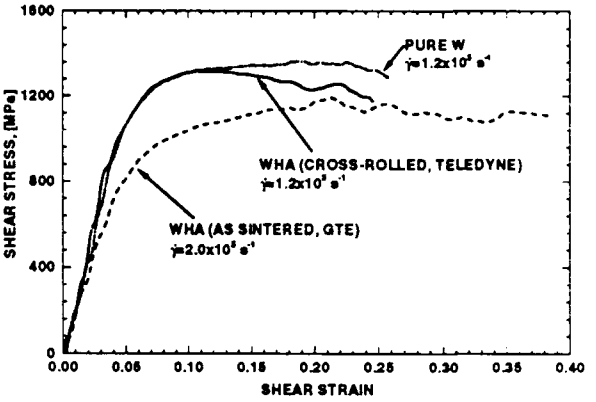

Fig. 8 DYNAMIC SHEAR STRESS-STRAIN CURVES OF WHA AND W OBTAINED BY PRESSURE-SHEAR PLATE IMPACT

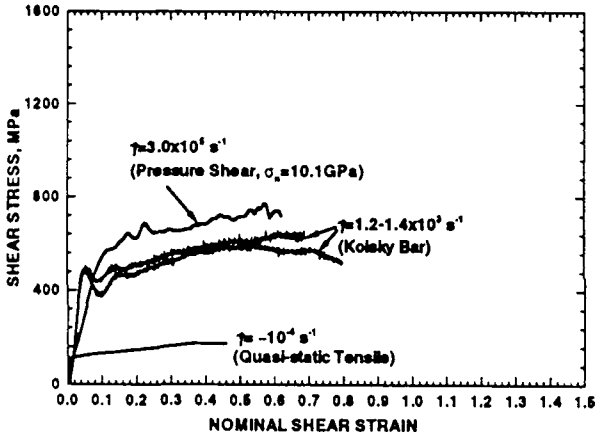

Fig. 9 STRESS-STRAIN RESPONSE OF MATRIX ALLOY

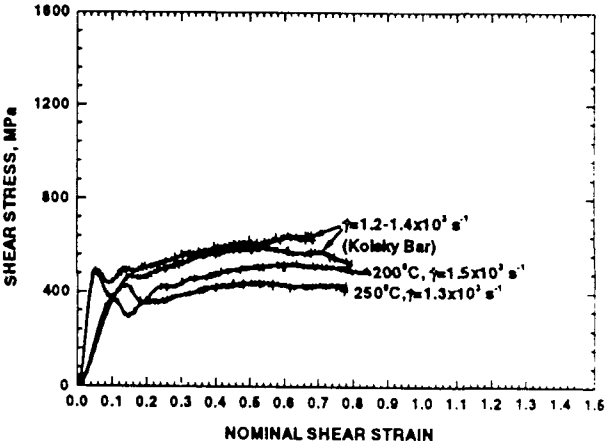

Fig. 10 TEMPERATURE DEPENDENCE OF STRESS-STRAIN RESPONSE FOR MATRIX ALLOY

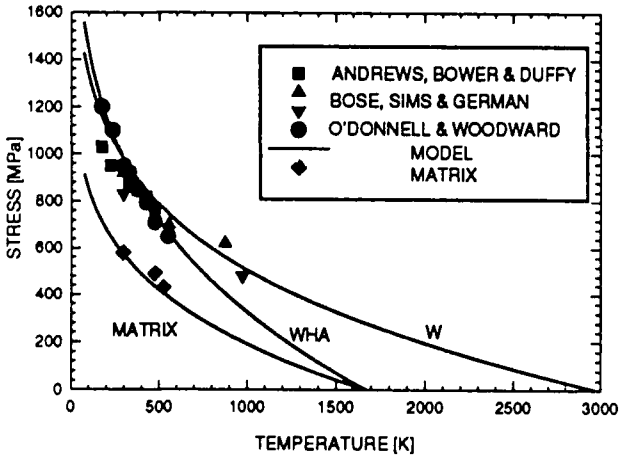

Fig. 11 TEMPERATURE DEPENDENCE OF FLOW STRESS FOR WHA, W AND MATRIX ALLOY

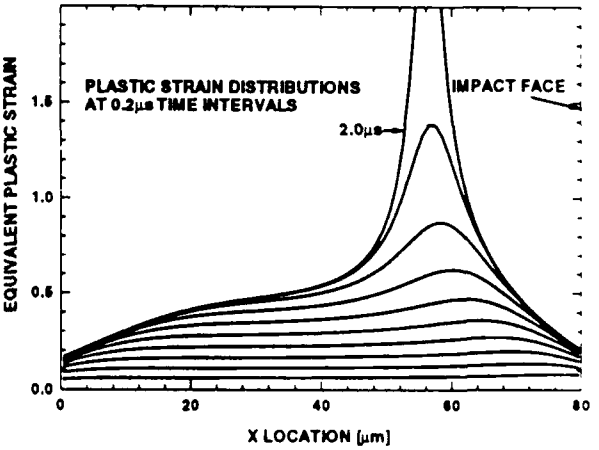

Fig. 12 CALCULATED PLASTIC STRAIN DISTRIBUTIONS

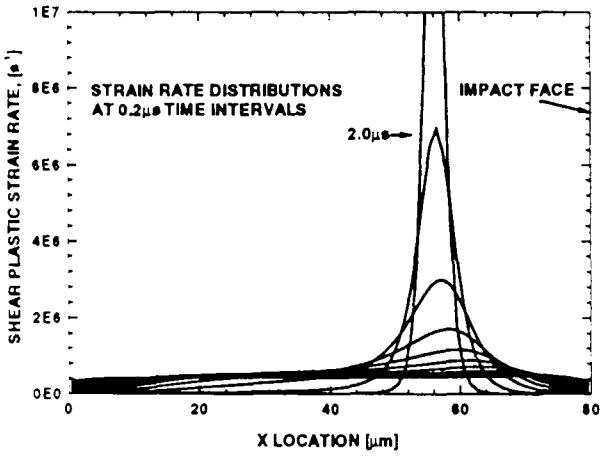

Fig. 13 CALCULATED STRAIN RATE DISTRIBUTIONS

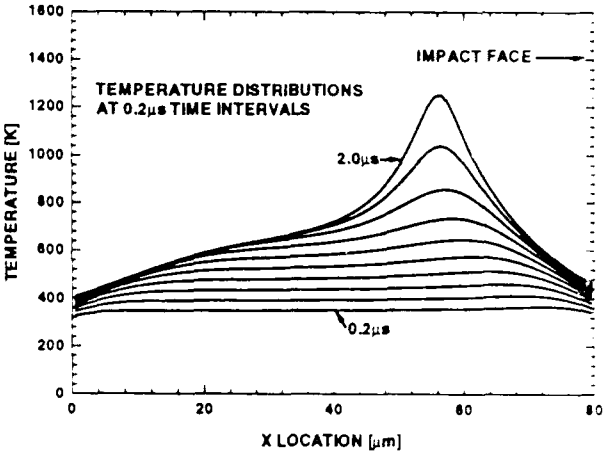

Fig. 14 CALCULATED TEMPERATURE DISTRIBUTIONS

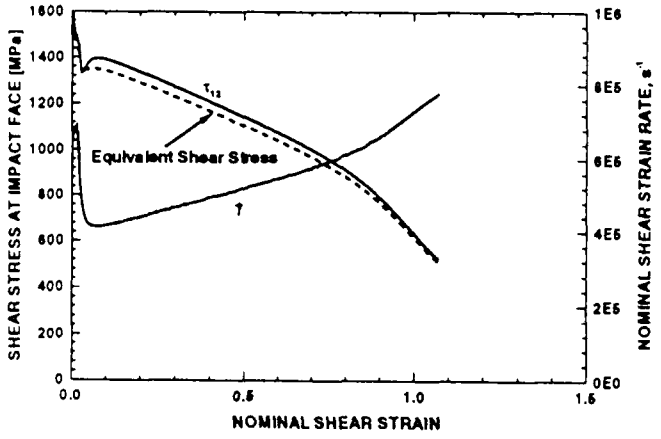

Fig. 15 CALCULATED STRESS-STRAIN CURVES AND NOMINAL SHEAR STRAIN RATE

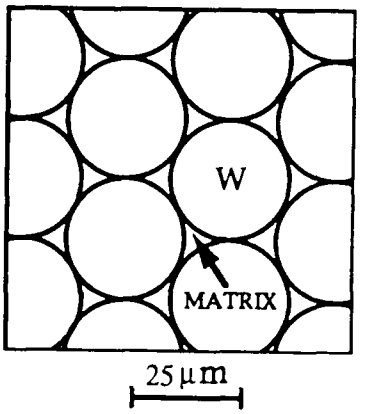

Fig. 16 UNDEFORMED CONFIGURATION

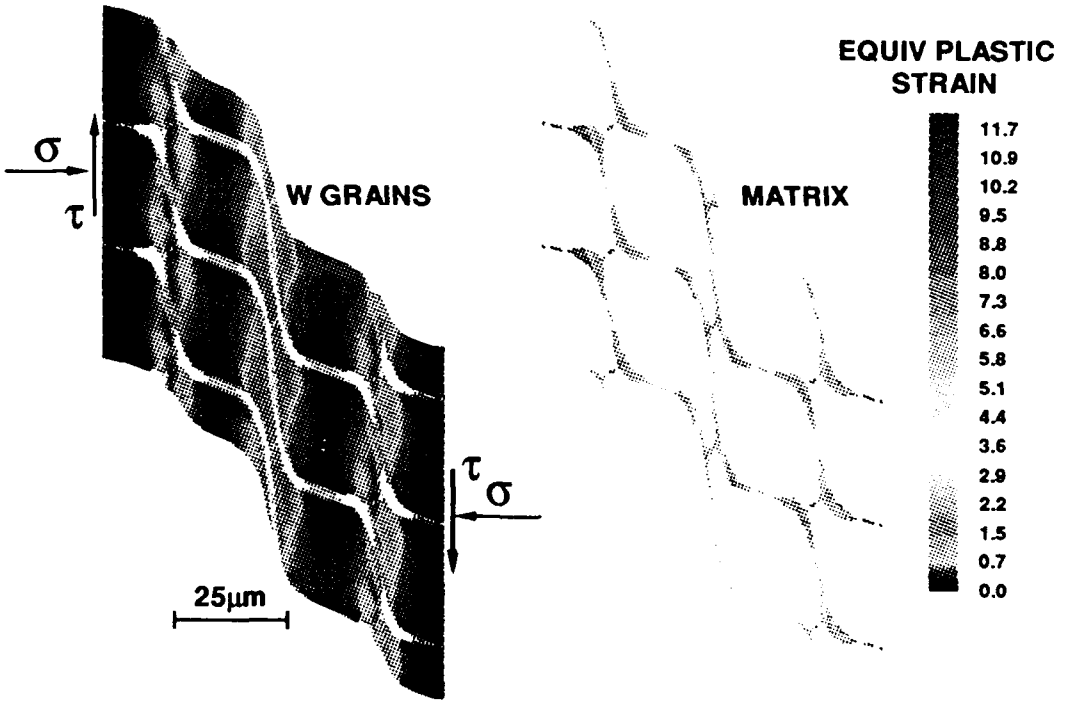

Fig. 17 EQUIVALENT PLASTIC STRAIN DISTRIBUTION 2μs AFTER IMPACT